Controlled Synthesis of Hierarchical Nickel and Morphology-Dependent Electromagnetic Properties

ARTICLE *in* THE JOURNAL OF PHYSICAL CHEMISTRY C · JANUARY 2010

Impact Factor: 4.77 · DOI: 10.1021/Jp908839r

8 AUTHORS, INCLUDING:

Charles Chenwei Wang
University of São Paulo
942 PUBLICATIONS **13,344** CITATIONS
SEE PROFILE

Ping Xu
Harbin Institute of Technology
102 PUBLICATIONS **2,251** CITATIONS
SEE PROFILE

Controlled Synthesis of Hierarchical Nickel and Morphology-Dependent Electromagnetic Properties

Chao Wang,[†] Xijiang Han,*[,†] Ping Xu,[†] Jingyu Wang,[†] Yunchen Du,[†] Xiaohong Wang,[‡] Wu Qin,[†] and Tao Zhang[†]

Chemistry Laboratory Center, Department of Chemistry, Harbin Institute of Technology, Harbin 150001, China, and Beijing Institute of Aeronautical Materials, Beijing 100095, China

Received: September 13, 2009; Revised Manuscript Received: January 9, 2010

Nickel nanomaterials with a wide range of morphologies and sizes, such as superfine nanoparticles, urchinlike chains, smooth chains, rings, and hexagonal Ni/Ni(OH)$_2$ heterogeneous structure plates, are synthesized in a single reaction system by simply adjusting the reaction conditions. The morphology transformation mechanism is systematically investigated. Magnetic measurement of urchinlike chains, smooth chains, and rings shows that the saturation magnetization (M_s) decreases with reduced sample size, and remanent magnetization (M_r) decreases with increasing reaction temperature. Additionally, coercivity (H_c) of urchinlike chains which is apparently larger than that of bulk nickel depends more on size than on shape anisotropy according to spherical chain reversal magnetization model. Enhanced microwave absorption of Ni/Ni(OH)$_2$ hexagonal plates compared with smooth chains and rings is due to the synergistic effect of magnetic loss and dielectric loss. Particularly, the urchinlike nickel chains exhibit a best absorption property in contrast with other as-synthesized samples and other reported nickel structures, which can be attributed to the geometrical effect, high initial permeability, point discharge effect, and multiple absorption. The prepared nickel nanomaterials can be applied as promising absorbing materials.

1. Introduction

Over the past years, there has been an increasing interest in developing hierarchically structural materials on a nanometer scale due to their novel or enhanced properties.[1−5] As a typical magnetic material, metal nickel has received much attention because of its potential applications in high-density magnetic recording, magnetic sensors, catalysis, and microwave absorption.[6−8] Consequently, a series of nickel nanostructural assemblies with different morphologies, including superfine nanoparticles (NPs), urchinlike chains, and nanorings were manufactured by various approaches.[9−16] For example, superfine nickel NPs were obtained by hydrazine reduction in ethylene glycol.[17] Three-dimensional (3D) urchinlike chains were usually synthesized by hydrothermal method or using external magnetic field under high temperature and high pressure or applying additional magnetization equipment.[18,19] Up to now, only a few pieces of literature have been concerned with the construction of nickel rings, though magnetic nanorings have drawn much attention for their unique closed structure.[20−27] A survey of literature indicated that only Ni−Co rings and Ni rings were reported, which were prepared by solvothermal method and hard-template method, respectively.[28,29] Of note is that these morphologies are fabricated under different complicated reaction systems. An easy realization of controlled synthesis and transformation of morphologies in a single system is still not available.

Nickel is a kind of widely used microwave absorbing material that would attenuate electromagnetic wave mainly by magnetic loss.[30−32] To date, most works on microwave absorbing behavior are focused on nickel superfine NPs; however, no attention has been paid to the morphology-dependent microwave absorbing properties.[17,33] In addition, recently there has been a tremendous increase in interest of core/shell heterogeneous structure materials that can achieve a synergistic effect of magnetic and dielectric loss to enhance absorbing ability.[34−41] Conventional core/shell heterogeneous structures are realized step by step, and a shell is usually constructed on a preprepared core, resulting in a long processing period and much cost.

Here, we demonstrate an easy approach to realizing the controlled synthesis of differently shaped nickel nanomaterials such as superfine NPs, urchinlike chains, smooth chains, rings, and hexagonal Ni/Ni(OH)$_2$ heterogeneous structure plates by simply adjusting reaction conditions in a single system at atmospheric pressure and no more than 85 °C without applying any external magnetic field and hard templates. To the best of our knowledge, this is the first time to report the assembly process of nickel from NPs of several nanometers to urchinlike chains of hundreds of nanometers, as well as the transformation from urchinlike chains to smooth chains. Furthermore, synthesis of nickel rings without hard templates and fast preparation of hexagonal Ni/Ni(OH)$_2$ heterogeneous structure plates are also original. The morphology transformation mechanism and morphology-dependent magnetic and electromagnetic properties have been investigated in detail.

2. Experimental Section

2.1. Materials. All chemicals used in this experiment were analytical grade and used without further purification. $NiCl_2 \cdot 6H_2O$, PVP K30, $N_2H_4 \cdot H_2O$ 80%, and ethylene glycol (EG) were purchased from Guangfu Chemical Co. Ltd. (Tianjin, China), and NaOH was purchased from Dalu Chemical Co. Ltd. (Tianjin, China).

2.2. Synthesis. Scheme 1 illustrates the reaction conditions for differently shaped samples. Superfine nickel NPs were

* Corresponding author. Tel.: +86-451-86413702. Fax: +86-451-86418750. E-mail: hanxj63@yahoo.com.cn.
[†] Harbin Institute of Technology.
[‡] Beijing Institute of Aeronautical Materials.

10.1021/jp908839r
Published on Web 01/29/2010

SCHEME 1: Flowchart for the Synthesis of Differently Shaped Samples

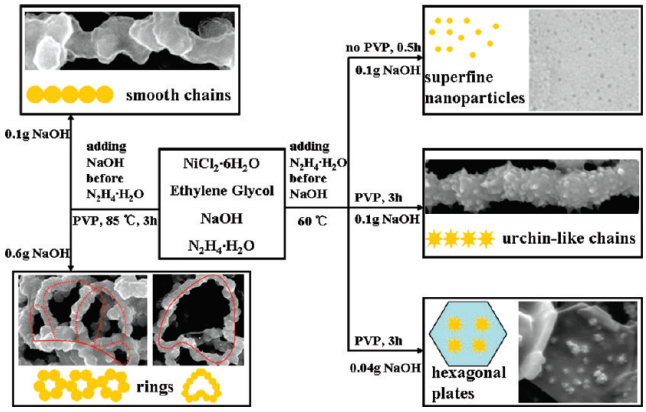

prepared by adding 0.0297 g of $NiCl_2·6H_2O$ into 22.5 mL of EG at 60 °C in a three-necked flask. After vigorous stirring for 15 min, 1.6 mL of $N_2H_4·H_2O$ was injected and 10 min later 0.1 g of NaOH was added, and then the reaction was maintained for another 0.5 h.[17]

Urchin-chain-like nickel was prepared by adding 0.125 g of PVP and 0.0297 g of $NiCl_2·6H_2O$ into 22.5 mL of EG at 60 °C. After vigorous stirring for 15 min, 1.6 mL of $N_2H_4·H_2O$ was injected and 10 min later 0.1 g of NaOH was added, and then the reaction was maintained for another 3 h.

Smooth nickel chains were synthesized by adding 0.125 g of PVP and 0.0297 g of $NiCl_2·6H_2O$ into 22.5 mL of EG at 85 °C. After vigorous stirring for 15 min, 0.1 g of NaOH was added and 10 min later 1.6 mL of $N_2H_4·H_2O$ was injected, and then the reaction was maintained for another 3 h.

Nickel rings were prepared by adding 0.125 g of PVP and 0.0297 g of $NiCl_2·6H_2O$ into 22.5 mL of EG at 85 °C. After vigorous stirring for 15 min, 0.6 g of NaOH was added and 10 min later 1.6 mL of $N_2H_4·H_2O$ was injected, and then the reaction was maintained for another 3 h.

Hexagonal Ni/$Ni(OH)_2$ heterogeneous structure plates would be obtained by adding 0.125 g of PVP and 0.0297 g of $NiCl_2·6H_2O$ into 22.5 mL of EG at 60 °C. After vigorous stirring for 15 min, 1.6 mL of $N_2H_4·H_2O$ was injected and 10 min later only 0.04 g of NaOH was added, and then the reaction was maintained for another 3 h.

After the reaction, the products were collected by centrifugation at 3000 rpm for 10 min and then washed with water nine times and with ethanol for the last time. Then the products were dried in a vacuum oven at 60 °C for 12 h.

2.3. Calculation. The most detailed experimental observations of the electronic structure have been performed for multilayers with 4−5 unit cell thick slabs.[42] Thus the original crystal layers Ni(100), Ni(110), and Ni(111) focused on this thickness. Periodic slabs based on the (4 × 4) surface unit cell were used in our calculations as a good compromise between the desire to reduce defect−defect interaction and computational limitations. Dynamic simulations were performed with a constant number of atom, temperature, and pressure in the ethylene glycol solution. The temperature was controlled in each system using Nose−Hoover chain thermostats.[43] The smooth particle mesh Ewald method was used to calculate the electrostatic interactions.[44] The real space part of the Ewald sum and the van der Waals interactions were truncated at 10 Å with a spherical truncation scheme. An integration time step of 1.0 fs was used in the simulations, and a 10.0 fs time step with multiple time step integration was selected for the simulations to balance the large system sizes with reasonable computational times. All bond lengths involving atoms of nickel layers were set to be free.

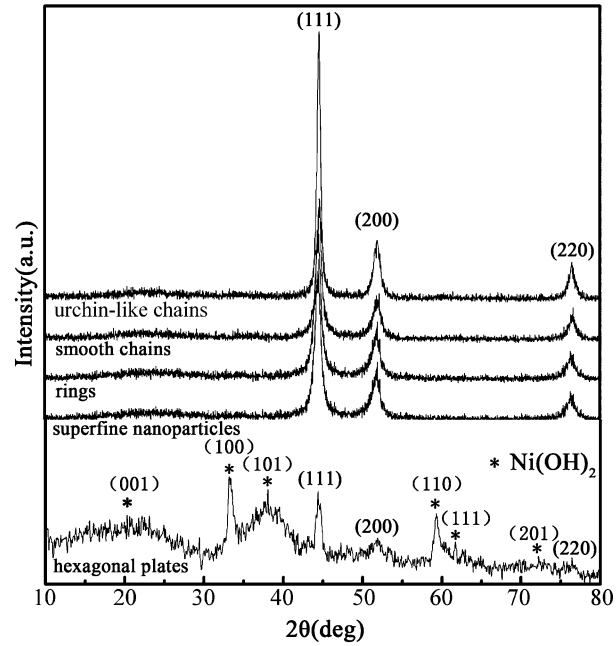

Figure 1. X-ray diffraction patterns of differently shaped samples.

2.4. Characterization. The morphologies of the samples were characterized by scanning electron microscopy (SEM, FEI SIRION) and transmission electron microscopy (TEM, FEI TECNAI G^2). The crystallite structures of the prepared samples were determined using an XRD-6000 X-ray diffractometer (Shimadzu) with a Cu Kα radiation source ($\lambda = 1.5405$ Å, 40.0 kV, 30.0 mA). The magnetic properties (intrinsic coercivity, saturation, and remanent magnetization) were measured using a vibrating sample magnetometer (VSM, Lake Shore 7307). A HP-5783E vector network analyzer was applied to determine the relative permeability and permittivity in the frequency range of 2−18 GHz for the calculation of reflection loss. A sample containing 60 wt % of obtained products was pressed into a ring with an outer diameter of 7 mm, an inner diameter of 3 mm, and a thickness of 2 mm for microwave measurement, in which wax was used as the binder.

3. Results and Discussion

Figure 1 presents the X-ray diffraction patterns of samples prepared under different conditions. All the diffraction peaks of differently shaped Ni (the images are listed in section 3.1) such as urchinlike chains, smooth chains, rings, and superfine NPs match well with the face-centered cubic (fcc) Ni crystal (JCPDS Card No. 04-0850), and the peaks located at 44.48°, 51.89°, and 76.53° can be indexed to (111), (200), and (220) planes. The sharp diffraction peaks of the as-synthesized Ni and no characteristic peaks due to impurities of nickel oxides and hydroxides indicate pure crystalline of good crystallinity. XRD peaks of hexagonal plates can be indexed as hexagonal $Ni(OH)_2$ (JCPDS Card No. 14-0117) and fcc nickel. The broad $Ni(OH)_2$ diffraction peaks such as (001), (101) show a poorly crystallized layered phase with a turbostratic disorder for the presence of Cl^- if nickel chloride was used as the nickel source.[16] The broad diffraction band of different samples at around $2\theta = 22°$ could be aroused from residual PVP.

3.1. Morphology. ***3.1.1. Superfine Nickel Nanoparticles and Urchinlike Chains.*** Superfine nickel NPs with sizes from 3 to 8 nm are formed after 0.5 h as shown in Figure 2a and can

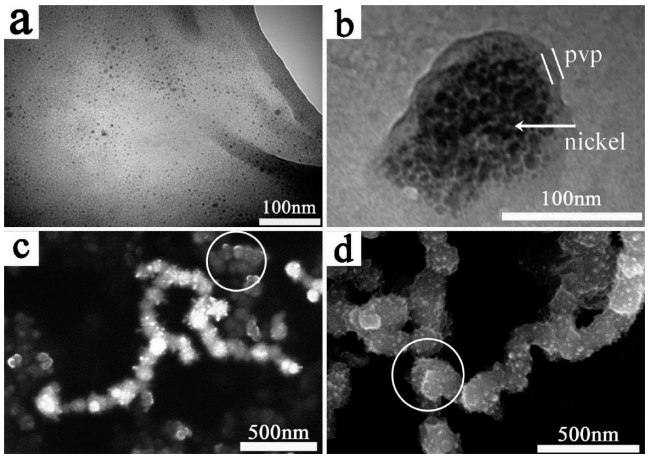

Figure 2. (a) TEM image of superfine nickel NPs after reaction for 0.5 h. TEM and SEM images of urchin-chain-like nickel synthesized at different reaction stages: (b) 0.5; (c) 1; (d) 3 h.

remain monodispersed even when the reaction time is prolonged to 3 h (image not displayed). However, the addition of PVP resulted in the agglomeration of superfine NPs to form urchinlike nickel chains. Figure 2b demonstrates a nanosphere covered by PVP consisting of nickel NPs of several nanometers to dozens of nanometers. Compared with Figure 2a, the particles size is enlarged and much of them agglomerate to form the nanosphere. When the reaction time is prolonged to 1 h, the primary urchin-chain-like nickel is formed (Figure 2c), while the nanosphere surface is not fully covered by the aciculae as shown in the circled region. Many superfine NPs are around nanospheres (Figure S1, Supporting Information) indicating that the self-assembly is not completed yet. However, high-yield urchinlike nickel chains can be achieved when the reaction period is extended to 3 h. A TEM image (Figure S2, Supporting Information) reveals visible interparticle spacing between adjacent particles and no superfine NPs locate nearby, which means the assembly is adequately completed. Figure 2d gives an SEM image of the urchinlike nickel with the sizes from 150 to 300 nm. Additionally, an apparently dead end of branches emerges in the circled area, and this phenomenon may often occur in Cayley Trees when two growing branches stumble upon each other.[15]

We believe that both $N_2H_4 \cdot H_2O$ and PVP play important roles in the growth of urchinlike nickel chains. Most probably, $N_2H_4 \cdot H_2O$ serves as the reducing agent while PVP molecules behave as soft templates. Herein we think the agglomerate of superfine NPs becomes a nanosphere (Figure 2b) under the effect of wrap of too much adsorbed PVP molecule chains. There is also a thermodynamic driving force for the agglomeration growth because the surface energy can be reduced substantially when the interface is eliminated. Then the nanospheres are arranged into chains driven by magnetic dipole interaction as time extended.[15]

3.1.2. Smooth Chains. It is found that the temperature and adding sequence of NaOH and $N_2H_4 \cdot H_2O$ have great influence on the final morphology of the products. Figure 3a shows that even when NaOH is added before $N_2H_4 \cdot H_2O$ at 60 °C, there are still some aciculae, but the aciculae are shorter than that in Figure 2d. When only the temperature is increased to 85 °C and $N_2H_4 \cdot H_2O$ is still added before NaOH, the aciculae of prepared chainlike nickel (Figure 3b) are much less and shorter in contrast with that in Figure 2d. If both the adding sequence and temperature are changed, smooth nickel chains with diameters of about 150 nm are obtained as shown in Figure 3c.

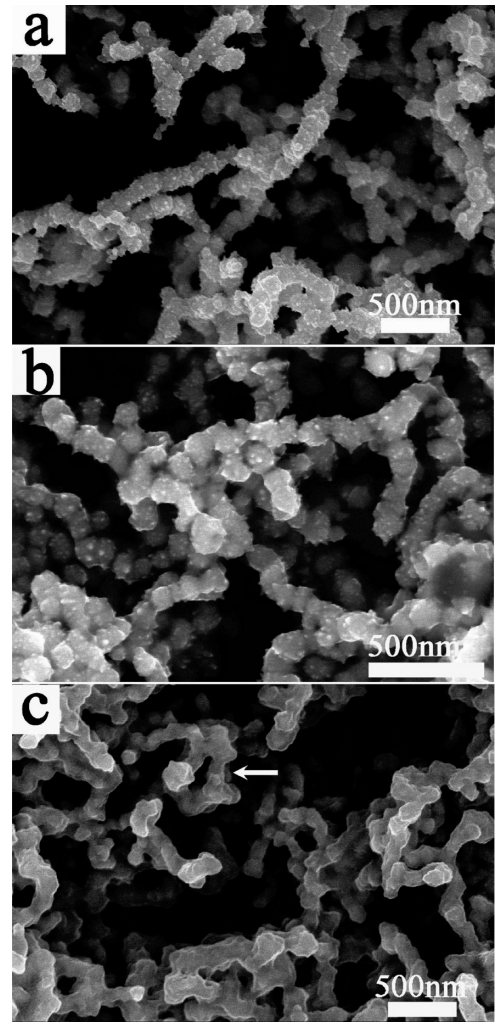

Figure 3. SEM images of chainlike nickel synthesized by (a) adding NaOH before $N_2H_4 \cdot H_2O$ at 60 °C, (b) adding $N_2H_4 \cdot H_2O$ before NaOH at 85 °C, (c) and adding NaOH before $N_2H_4 \cdot H_2O$ at 85 °C (smooth nickel chains are synthesized).

Herein, we can conclude that although the temperature and adding sequence of $N_2H_4 \cdot H_2O$ and NaOH both can control the morphology of nickel chains, the former is much more important. It is worth noting that a few rings emerge as indicated by the arrow in Figure 3c.

Generally, the evolution of a solid from liquid involves two fundamental steps such as nucleation and growth. If $N_2H_4 \cdot H_2O$ is added before NaOH, the chemical bond between Ni^{2+} and N_2H_4 forms before the reduction, which influences the growth rate of some crystal faces resulting in the anisotropic growth from the nuclei, and finally the urchinlike morphology is formed.[9] On the contrary, the chemical bond between Ni^{2+} and N_2H_4 could not be formed by adding $N_2H_4 \cdot H_2O$ after NaOH because the bond energy between OH^- and Ni^{2+} is larger than that between N_2H_4 and Ni^{2+}. However, Li and co-workers have reported just the contrary conclusion that urchinlike nickel is preferably formed at high temperature if using absolute alcohol as solvent.[9] Materials Studio 4.3 software is applied in order to reveal the influence mechanism of temperature. A growth scheme of different crystal planes of Ni is illustrated in Figure 4. On the surfaces of Ni(100), Ni(110), and Ni(111), nickel atoms are attracted to be filled into the lattice points of crystal planes with Molecule Dynamic (MD) simulation time. After 1 ns, two new crystal planes (the number of yellow planes increased by two) grow on the surface of the original Ni(100),

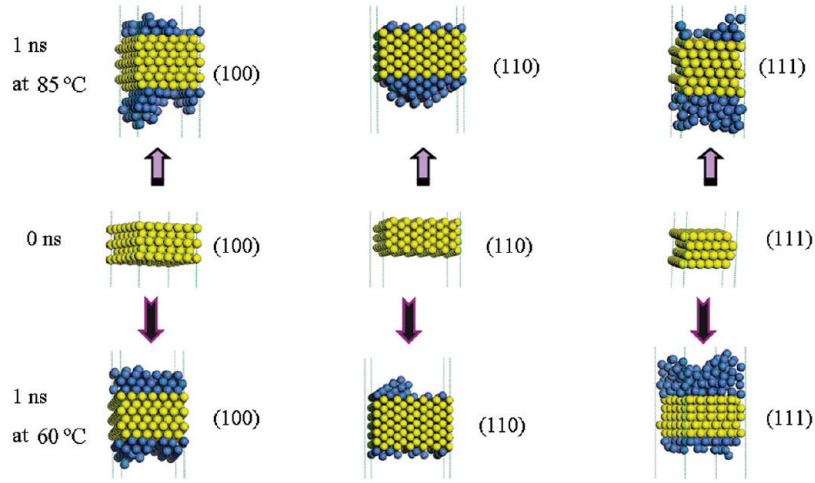

Figure 4. Crystal growth at different temperatures after 1 ns MD simulation. Yellow spheres symbolize the well crystallized atoms that packed at the lattice point, while the blue spheres are the irregularly packed atoms.

Ni(110), and Ni(111) crystal layers at 85 °C, which means the growth rates of the three crystal planes are almost the same. However, after 1 ns at 60 °C, only one new crystal layer grows on Ni(100) and Ni(111), respectively, while four new layers are obtained on the original Ni(110), implying there is a preferred direction which may be responsible for the growth of aciculae. The different conclusion between our research and Li's may be attributable to different solvents, because the dielectric constant of solution could change the surface energy of newly produced nickel.[11]

3.1.3. Rings. Figure 5a shows a typical SEM image of nickel nanorings which clearly indicates that every ring consists of several dozens of nanospheres with diameters ranging from 150 to 200 nm. The surface of the rings is a little rougher compared with smooth chains but not as rough as the urchinlike chains. The individual nanospheres are spaced fully together and finally form the flux-closure ring that can be illustrated by a dipole-directed assembly mechanism.[22] A closed ring where all dipoles could be located in a circuit will be helpful to decrease the magnetostatic energy and spontaneous magnetostatic field, and thus the rings could be prepared by the degradation of dipoles in the manner of interaction between the unpaired end dipoles of two or several chains. It is noted that rings in Figure 5a are linearly linked and overlapped, and this may be because some nanorings with the same magnetostatic direction, clockwise or counterclockwise, are easily linked together by a second magnetostatic field that would induce self-assembly, and finally a long chain made up of nanorings is formed.[23] Figures 5b and 5c show the peculiar morphology of B-shaped and heart-shaped rings, respectively. The formation mechanism of these kind of anamorphic rings can be illustrated by consulting the similar Fe_3O_4 heart-shaped rings that form because of screening of dipolar interactions which weakens the force between opposite ring parts considerably.[24] Actually, if the nickel particles labeled "I" and "II" in Figure 5b are attached together, a chain consisting of two linearly linked rings would be formed as that in Figure 5a.

Compared with the preparation of smooth chains, we can get rings simply by increasing NaOH from 0.1 to 0.6 g. This is based on the previous report that the dipolar−dipolar interactions between two magnetic particles scaled as r^6/σ^3, where r is the particle radius and σ consists of the particle diameter and the thickness of the nonmagnetic layer.[26] The connected particles in a ring and larger size compared with smooth chains result in smaller σ and larger r, leading to strong magnetic dipoles

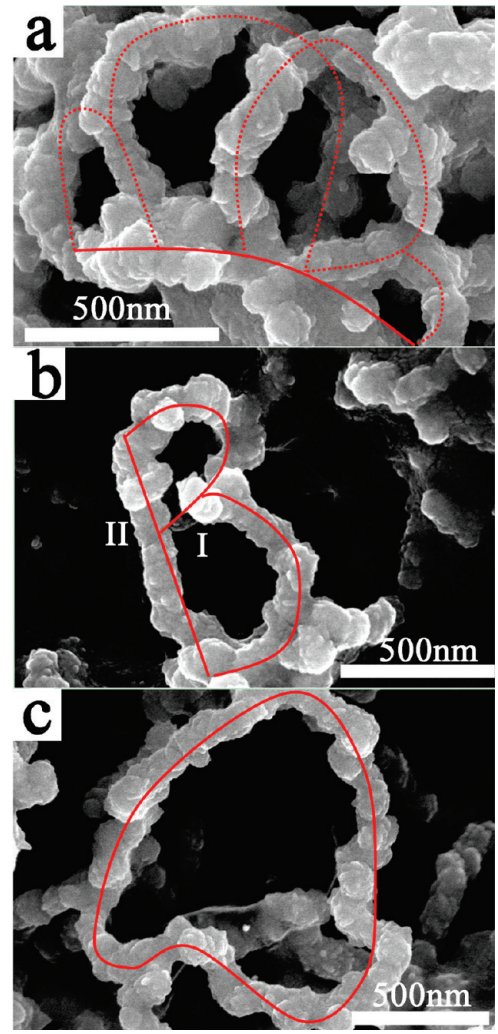

Figure 5. SEM images of anamorphic nickel rings.

interaction to overcome the potential barrier that involves an energetic cost for bending chains.[27] Furthermore, it is revealed that NaOH not only increases the pH value of solution in order to enhance the reduction ability of N_2H_4 but also serves as catalyst.[17] Namely, the increased NaOH content would accelerate reaction rate, leading to the fast formation of short chains with disordered magnetostatic direction. The tendency to form rings

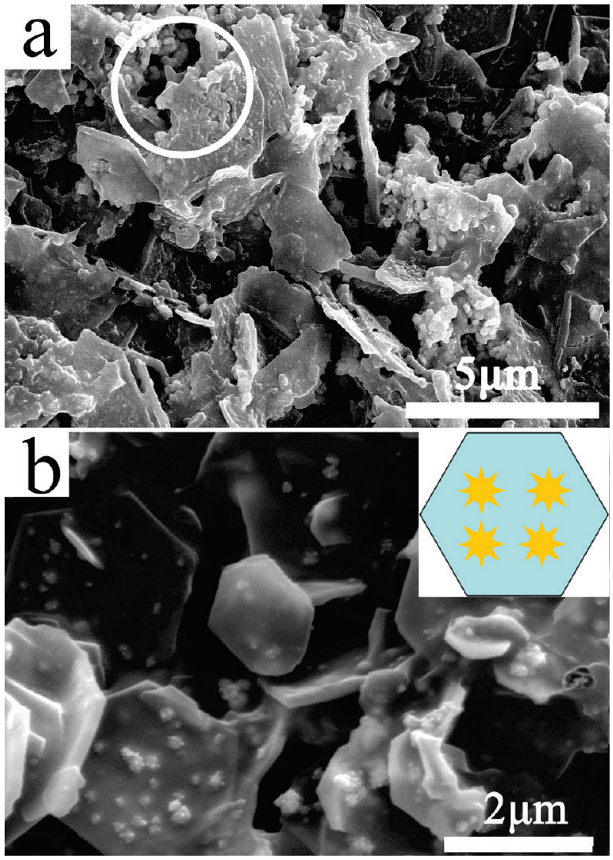

Figure 6. SEM images of hexagonal Ni/Ni(OH)$_2$ plates after reaction for (a) 1.5 h and (b) 3 h (the right inset is the scheme of hexagonal Ni/Ni(OH)$_2$ heterogeneous structure plate).

in order to decrease the magnetostatic energy and the outside field is more obvious for these disordered short chains.[28]

3.1.4. Hexagonal Ni/Ni(OH)$_2$ Heterogeneous Structure Plates. Figure 6a shows the urchinlike nickel particles partially encapsulated in Ni(OH)$_2$ hexagonal plates. We think urchinlike Ni would be prepared with priority, and then because of insufficient catalyst NaOH, Ni^{2+} cannot be completely reduced and Ni(OH)$_2$ is obtained on the surface of Ni. At this stage, Figure 6a reveals many discrete particles as indicated in the circle as well as lots of fragmentary hexagonal plates coexisting and no integrated plates being produced. After the reaction continues for 3 h, Ni/Ni(OH)$_2$ heterogeneous structure particles are connected together into integrated hexagonal plates as shown in Figure 6b by the intrinsic crystal orientation of Ni(OH)$_2$.[10] It should be noted that only Ni(OH)$_2$ hexagonal plates could be obtained if the amount of NaOH was decreased to 0.03 g, with other reaction conditions remaining the same as the preparation of Ni/Ni(OH)$_2$ hexagonal plates (Figure S3, Supporting Information). This further confirms that the hexagonal plates in Figure 6b are Ni(OH)$_2$, and the particles embedded are Ni.

Ni is a kind of widely used magnetic loss microwave absorbing material, while Ni(OH)$_2$ is a kind of dielectric loss microwave absorbing material.[41] As mentioned above, traditional methods to construct microwave absorption materials with heterogeneous structures in order to realize synergistic effect of magnetic loss and dielectric loss are not time- and cost-effective. The facile synthesis of Ni/Ni(OH)$_2$ heterogeneous composites that combine materials with different loss mechanisms by only one step within 3 h may be valuable in microwave absorption application.

To this end, our efforts herein would serve as the first attempt of this type of systematic investigation for nickel hierarchical

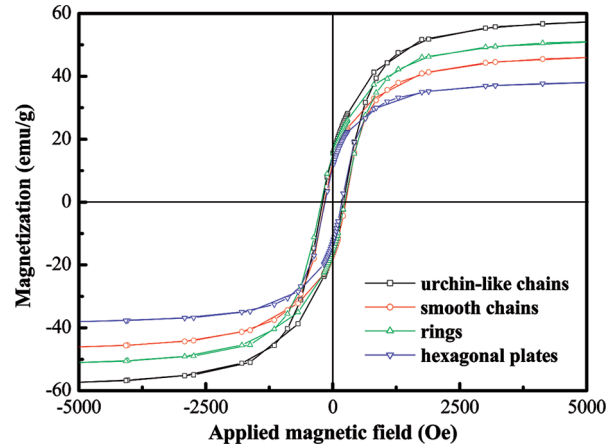

Figure 7. Magnetic hysteresis ($M-H$) loops measured at room temperature for four samples.

nanomaterials, and thus a great picture for the chemical conversation of this materials family has been summarized in Scheme 1.

3.2. Magnetic Properties. It is known that the magnetic properties of nanomaterials are strongly dependent on their size and morphology. The magnetic hysteresis ($M-H$) loops and electromagnetic parameters of superfine nickel NPs are not measured because they are superparamagnetic and exhibit extremely poor microwave absorbing ability with the maximum reflection loss nearly 0 dB.[35] Figure 7 shows $M-H$ loops of four different morphology samples. The coercivities (H_c) measured are 204.90, 215.73, 210.31, and 142.84 Oe, and the corresponding saturation magnetizations (M_s) are about 59.39, 47.72, 52.79, and 39.23 emu/g and remanent magnetizations (M_r) are 15.16, 15.07, 14.05, and 10.46 emu/g for urchinlike chains, smooth chains, rings, and hexagonal plates, respectively. The M_s, M_r, and H_c are lowest for hexagonal plates due to the presence of nonmagnetic Ni(OH)$_2$. Apparently, though a residua of nonmagnetic PVP is present, both M_s and H_c of urchinlike chains are greatly enhanced compared with the reported urchinlike nickel chains synthesized by other methods.[12−14,40] Furthermore, H_c, M_r of above four samples and M_s of urchinlike nickel are evidently improved in comparison with bulk nickel (0.7 Oe, 2.7 emu/g, 55 emu/g).[19]

Generally, M_s for nanoscale magnetic material is lower than that for bulk material because of spin disorder on the surface; in other words, M_s decreases as the size is reduced. Additionally, M_r will decrease with increasing temperature due to thermal activation effect.[30] Accordingly, it is reasonable to accept that M_s values of smooth chains are lower than those of rings and much lower than those of urchinlike chains, and M_r of smooth chains and rings synthesized at 85 °C are lower than those of urchinlike nickel prepared at 60 °C. However, it is still hard to understand that M_s for the nanoscale urchinlike chains is higher than that for bulk nickel (55 emu/g). As a matter of fact, this surprising phenomenon is reported in the synthesis magnetic materials such as Ni and $BaFe_{12}O_{19}$ and can be explained by the fact that the magnetic easy axis of acicular Ni nanocrystallites is aligned along the long axis of the chains whose orientation is greatly influenced by the magnetic field of surrounding nickel, and eventually the M_s is improved.[31,40]

Urchinlike chains with large aspect ratio should have the highest H_c for their obvious shape anisotropy; however, it is lower than that of smooth chains and rings. In order to illustrate the H_c of differently shaped samples, the spherical chain reversal magnetization model is applied.[32] With the fanning model, the H_c measured along the chains is expressed as

$$H_{c_n} = \frac{\mu}{R^3}(6K_n - 4L_n) \quad (1)$$

$$K_n = \sum_{j=1}^{n} \frac{(n-j)}{nj^3} \quad (2)$$

$$L_n = \sum_{j=1}^{1/2(n-1)<j\leq 1/2(n+1)} \frac{[n-9(2j-1)]}{n(2j-1)^3} \quad (3)$$

where n, μ, and R are the number of spherical particles in a chain and dipole moment and the diameter of each sphere, respectively. We can utilize this model to calculate H_c by M_s. The term μ/R^3 can be expressed using saturation magnetization per unit volume M_s, as $\mu/R^3 = (\pi/6)M_s$. Thus, by using experimental M_s of urchin-chain-like nickel and assuming $n = 10$, we obtain the value of H_c as 195.45 Oe. This value can further be modified by considering the correction factor which is 1.1 for randomly oriented effect in a powdered sample.[30,34] Then we get the final $H_c' \sim 1.1H_c = 214.99$ Oe, which agrees well with the experimental value 204.90 Oe within 4.92%. From another point of view, a smaller diameter would lead to a larger H_c by eq 1, and that is why the H_c of smooth chains is a little larger than that of rings and much larger than that of urchinlike chains. That is to say, H_c depends more on sample size than on shape anisotropy.

For the application in microwave absorption, the initial permeability (μ_i) of an absorber should be as high as possible, and the permeability of ferromagnetic materials can be expressed as

$$\mu_i = M_s^2/(akH_cM_s + b\lambda\xi) \quad (4)$$

where a and b are two constants determined by the material composition, λ is the magnetostriction constant, and ξ is an elastic strain parameter of the crystal.[37] It can be seen from the above equation that both higher M_s and lower H_c are favorable to the improvement of the μ_i value, which in turn would enhance the microwave absorption. Thus, the urchinlike Ni chains with high μ_i imply that it would be a promising excellent microwave absorber.

3.3. Electromagnetic Parameters and Microwave Absorption. The real parts of relative complex permittivity and permeability symbolize the storage ability of electromagnetic energy, while the imaginary parts represent the loss ability. Figure 8 reveals that ε'' is positive in the whole range 2−18 GHz, while μ'' is also positive for greatest frequency range. Therefore, dielectric loss and magnetic loss occur simultaneously for four samples. A surprising phenomenon that μ'' of hexagonal plates with nonmagnetic $Ni(OH)_2$ is larger than those of other three nickel samples in most frequency range occurs, which may need further investigation.

As we know, the positive μ'' is often used to manifest energy loss for magnetic materials, while a negative μ'' value means the magnetic energy is radiated out with no absorption. Though nickel is universally considered as a magnetic loss material, μ'' becomes negative from 8.5 GHz for smooth chains and from 13 GHz for the other three samples. However, based on the measured data of permittivity and permeability, the reflection loss (RL) usually can be evaluated by the following equation:

$$RL = 20\log|(Z_{in} - Z_0)/(Z_{in} + Z_0)| \quad (5)$$

where Z_0 is the impedance of free space and Z_{in} is the input characteristic impedance, which can be expressed as

$$Z_{in} = Z_0\sqrt{(\mu_r/\varepsilon_r)}\tanh\{j(2\pi fd/c)\sqrt{\mu_r\varepsilon_r}\} \quad (6)$$

where c is the velocity of light, f is frequency, and d is the thickness of an absorber. The reflection loss (RL) of the four samples is shown in Figure 9.

Though smooth chains with the lowest μ'' and rings with the lowest ε'' show poor microwave absorption as indicated in Figure 9, they exhibit a little improved absorbing ability when the strongest absorption reaches nearly −5 dB compared with the reported superfine NPs and flowerlike nickel with the strongest absorption no more than −4 dB.[33,35] Besides, the absorbing ability of $Ni/Ni(OH)_2$ hexagonal plates is much more enhanced, which may be due to the lag of polarization between Ni and $Ni(OH)_2$ interfaces as well as the synergistic effect of magnetic loss and dielectric loss. It is worth noting that both ε'' and μ'' of urchinlike chains are smaller than those hexagonal plates, but the RL of the former are much stronger with a peak −25.29 dB at 9.6 GHz. As a matter of fact, besides the dielectric loss and magnetic loss, the electromagnetic wave can be absorbed via the "geometrical effect", which means that when the thickness of absorber satisfies the equations

$$d = l\lambda_m/4(l = 1, 3, 5,...) \quad (7)$$

$$\lambda_m = \lambda_0/(|\mu_r||\varepsilon_r|)^{1/2} \quad (8)$$

where the incident and reflected waves in the absorber are out of phase 180°. Consequently, the reflected waves in the air−absorber interface are totally canceled. In the above equation, λ_m is the wavelength at certain frequency, $|\mu_r|$ and $|\varepsilon_r|$ are the moduli of μ_r and ε_r, respectively, and λ_0 is the wavelength in the free space.[36] We think a geometrical effect plays an important role in microwave absorption of urchinlike chains. At matching frequency $f_m = 9.6$ GHz, $\varepsilon_r = 16.95 - j4.35$, and $\mu_r = 0.94 - j0.06$. Substituting these values into eq 7 with $l = 1$, we get $d = 1.93$ mm, which is close to a thickness of 2 mm in our measurement. Therefore, the above calculations validate that the excellent microwave absorbing ability for urchinlike chains arises not only from dielectric loss and magnetic loss but also from geometrical effect.

On the other hand, we can deduce the urchinlike chains with strong absorbing ability qualitatively from its microscopic structure as shown in the right inset of Figure 9. As we all know, the acicular metal is commonly used as a lightning rod to attract lightning, and the wall in a microwave darkroom used for electromagnetic measurement consists of a cone-shaped absorber. Similarly, owing to the large aspect ratio of the aciculae, the charge concentration at the tips is distinctly concentrated when under an electromagnetic field. Thus, it is reasonable that the concentrated tips will act as multipoles that will be tuned with the incident microwaves for the point discharge effect and the energy is induced into dissipative current which leads to energy attenuation by the numerous conductive networks, resulting in strong absorption just as the action mechanism of lightning rod to lightning. In addition, the microwave would be multiscattered in the presence of aciculae, which results in repeated absorption. Meanwhile, the large exposed surface of

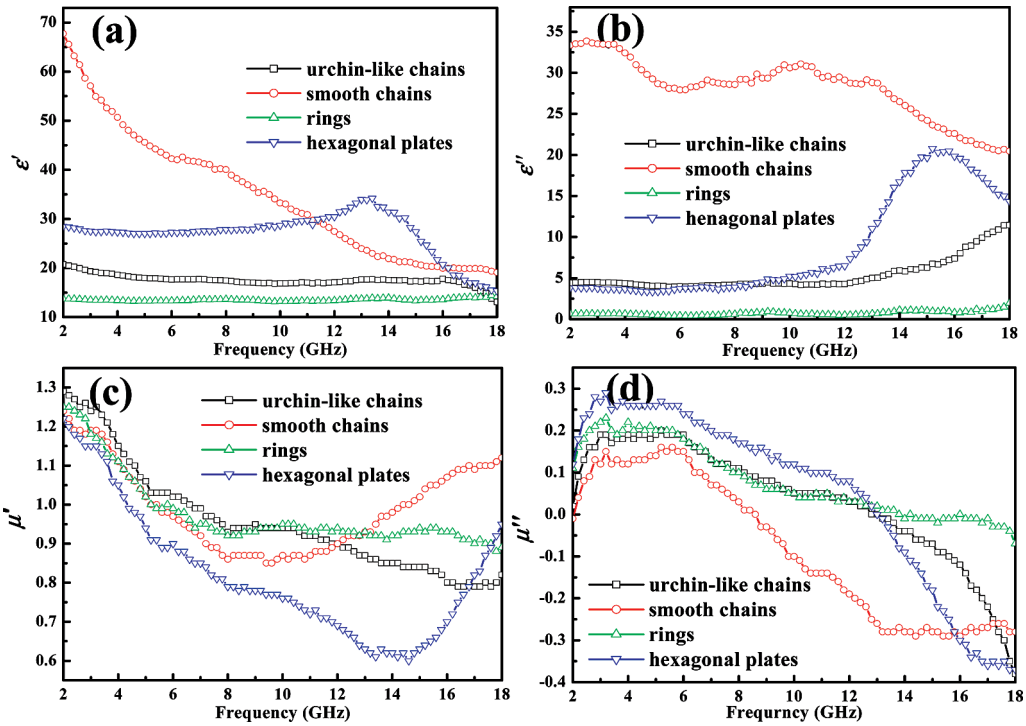

Figure 8. Electromagnetic parameters of the four differently shaped samples in the frequency range of 2−18 GHz: (a) real and (b) imaginary parts of relative complex permittivity; (c) real and (d) imaginary parts of the relative complex permeability.

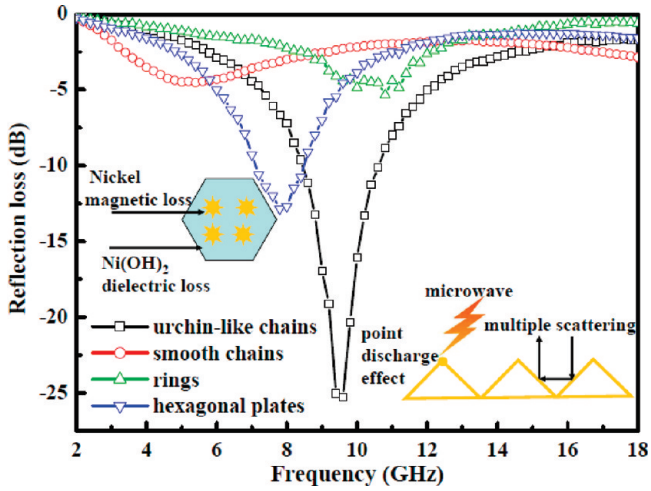

Figure 9. Reflection loss of differently shaped samples in the frequency range 2−18 GHz with the samples thickness of 2 mm. The left inset is the scheme of hexagonal Ni/Ni(OH)$_2$ heterogeneous structure plates that combines different loss mechanisms. The right inset is the qualitative illustration scheme of how microcosmic structure of urchinlike chains acts on electromagnetic wave and enhances absorbing ability.

aciculae would lead to increasing interfacial magnetic dipole polarization which may enhance magnetic loss.

Based on our previous work, nickel and conducting polymer complex can exhibit preferable microwave absorbing ability due to the synergistic effect of magnetic loss and dielectric loss, although nickel shows very poor microwave absorbing ability with the strongest RL no more than −4 dB.[33] However, the as-prepared urchinlike nickel chain exhibits a much better RL property, implying its application as an excellent microwave absorber if coated with other dielectric loss materials. Further experiment is undergoing.

4. Conclusion

In summary, we have successfully synthesized nickel nanomaterials with different morphologies such as superfine NPs, urchinlike chains, smooth chains, and rings, as well as hexagonal Ni/Ni(OH)$_2$ heterogeneous plates, in a single reaction system by simply modulating reaction conditions at atmospheric pressure and no more than 85 °C, without external magnetic field and hard template. Also, the morphology transformation mechanism is investigated in detail by exploring the influence of reaction time, sequence of adding agent, and temperature with the help of materials studio 4.3 software. The M_s value decreases as the particle size decreases owing to the spin disorder on the surface while M_r decreases with increasing temperature due to thermal activation effect. The spherical chain reversal magnetization model is applied to successfully illustrate that H_c depends more on size than on shape anisotropy, and the calculated value by this model agrees well with the experimental value. Hexagonal Ni/Ni(OH)$_2$ plates show stronger microwave absorption than smooth chains and rings due to the synergistic effect and interface polarization. It is noted that the urchinlike nickel chain may be a promising excellent absorber as it exhibits the best absorption property with a peak of −25.29 dB at 9.6 GHz in contrast with other as-synthesized samples and other nickel reported, and the absorbing mechanism can be illustrated by geometrical effect quantitatively as well as by high initial permeability, point discharge effect, and multiple absorption qualitatively.

Acknowledgment. This research is supported by the National Natural Science Foundation of China (No. 20776032). We thank C. C. Ke (Dalian Institute of Chemical Physics, Chinese Academy of Sciences) as well as S. Y. Shen (The Hong Kong University of Science and Technology, China) for the helpful discussion.

Supporting Information Available: TEM images of inadequately reacted and adequately reacted urchin-chain-like nickel.

This material is available free of charge via the Internet at http://pubs.acs.org.

References and Notes

(1) Ni, X. M.; Zhao, Q. B.; Zhang, D. E.; Zhang, X. J.; Zheng, H. G. *J. Phys. Chem. C* **2007**, *111*, 602.

(2) Zou, G. F.; Yang, H.; Jain, M.; Zhou, H. H.; Williams, D.; Zhou, M.; McCleskey, T.; Burrell, A.; Jia, Q. X. *Carbon* **2009**, *47*, 933.

(3) Erb, R. M.; Son, H. S.; Samanta, B.; Rotello, V. M.; Yellen, B. B. *Nature* **2009**, *457*, 999.

(4) Lu, X. B.; Zou, G. F.; Li, J. H. *J. Mater. Chem.* **2007**, *17*, 1427.

(5) Gao, Y. Q.; Wang, Z. H.; Wan, J. X.; Zou, G. F.; Qian, Y. T. *J. Cryst. Growth* **2005**, *279*, 415.

(6) Zinchenko, A. A.; Yoshikawa, K.; Baigl, D. *Adv. Mater.* **2005**, *17*, 2820.

(7) Bagkar, N.; Choudhury, S.; Bhattacharya, S.; Yakhmi, J. V. *J. Phys. Chem. B* **2008**, *112*, 6467.

(8) McFadden, S. X.; Mishra, R. S.; Valiev, R. Z.; Zhilyaev, A. P.; Mukherjee, A. K. *Nature* **1999**, *398*, 684.

(9) Ma, F.; Li, Q.; Huang, J. J.; Li, J. G. *J. Cryst. Growth* **2008**, *310*, 3523.

(10) Hu, W. B.; Zhao, Y. M.; Liu, Z. L.; Dunnill, C. W.; Gregory, D. H.; Zhu, Y. Q. *Chem. Mater.* **2008**, *20*, 5663.

(11) Wang, D. P.; Sun, D. B.; Yu, H. Y.; Meng, H. M. *J. Cryst. Growth* **2008**, *310*, 1198.

(12) An, Z. G.; Pan, S. L.; Zhang, J. J. *J. Phys. Chem. C* **2009**, *113*, 1347.

(13) Wang, Y.; Zhu, Q. S.; Zhang, H. G. *Mater. Res. Bull.* **2007**, *42*, 1450.

(14) Chen, Z.; Cao, M. H.; He, X. Y. *Chem. Lett.* **2008**, *37*, 736.

(15) Liu, C. M.; Guo, L.; Wang, R. M.; Deng, Y.; Xu, H. B.; Yang, S. H. *Chem. Commun.* **2004**, *23*, 2727.

(16) Xu, L. P.; Ding, Y. S.; Chen, C. H.; Zhao, L. L.; Rimkus, C.; Joesten, R.; Suib, S. L. *Chem. Mater.* **2008**, *20*, 313.

(17) Wu, S. H.; Chen, D. H. *J. Colloid Interface Sci.* **2003**, *259*, 283.

(18) Jia, F. L.; Zhang, L. Z.; Shang, X. Y.; Yang, Y. *Adv. Mater.* **2008**, *20*, 1050.

(19) Jiang, C. L.; Zou, G. F.; Zhang, W. Q.; Yu, W. C.; Qian, Y. T. *Mater. Lett.* **2006**, *60*, 2319.

(20) Liang, Z. H.; Zhu, Y. J.; Hu, X. L. *J. Phys. Chem. B* **2004**, *108*, 3490.

(21) Ohara, P. C.; Gelbart, W. M. *Langmuir* **1998**, *14*, 3418.

(22) Xiong, Y.; Ye, J.; Gu, X. Y.; Chen, Q. W. *J. Phys. Chem. C* **2007**, *111*, 7001.

(23) Tripp, S. L.; Dunin-Borkowski, R. E.; Wei, A. *Angew. Chem., Int. Ed.* **2003**, *42*, 5591.

(24) Philipse, A. P.; Maas, D. *Langmuir* **2002**, *18*, 9981.

(25) Guo, L.; Liang, F.; Wang, N.; Kong, D. S.; Wang, S. M.; He, L.; Chen, C. P.; Meng, X. M.; Wu, Z. Y. *Chem. Mater.* **2008**, *20*, 5165.

(26) Rosensweig, R. E. *Ferrohydrodynamics*; Cambridge University Press: Cambridge, U.K., 1985.

(27) Safran, S. A. *Nat. Mater.* **2003**, *2*, 71.

(28) Hu, M. J.; Lu, Y.; Zhang, S.; Guo, S. R.; Lin, B.; Zhang, M.; Yu, S. H. *J. Am. Chem. Soc.* **2008**, *130*, 11607.

(29) Duan, G. T.; Cai, W. P.; Luo, Y. Y.; Li, Z. G.; Lei, Y. *J. Phys. Chem. B* **2006**, *110*, 15729.

(30) Zhou, W.; Zheng, K.; He, L.; Wang, R. M.; Guo, L.; Chen, C. P.; Han, X. D.; Zhang, Z. *Nano Lett.* **2008**, *8*, 1150.

(31) Wang, C.; Han, X. J.; Xu, P.; Wang, X. H.; Li, X. A.; Zhao, H. T. *J. Alloys Compd.* **2009**, *476*, 563.

(32) Jacobs, I. S.; Bean, C. P. *Phys. Rev.* **1955**, *100*, 1062.

(33) Xu, P.; Han, X. J.; Wang, C.; Zhou, D. H.; Lv, Z. S.; Wen, A. H.; Wang, X. H.; Zhang, B. *J. Phys. Chem. B* **2008**, *112*, 10443.

(34) He, L.; Zheng, W. Z.; Zhou, W.; Du, H. L.; Chen, C. P.; Guo, L. *J. Phys.: Condens. Matter* **2007**, *19*, 036216.

(35) Lee, C. C.; Chen, D. H. *Appl. Phys. Lett.* **2007**, *90*, 193102.

(36) Deng, L. J.; Han, M. G. *Appl. Phys. Lett.* **2007**, *91*, 023119.

(37) Lv, R. T.; Cao, A. Y.; Kang, F. Y.; Wang, W. X.; Wei, J. Q.; Gu, J. L.; Wang, K. L.; Wu, D. H. *J. Phys. Chem. C* **2007**, *111*, 11479.

(38) Che, R. C.; Peng, L. M.; Duan, X. F.; Chen, Q.; Liang, X. L. *Adv. Mater.* **2004**, *16*, 401.

(39) Wang, J. C.; Xiang, C. S.; Liu, Q.; Pan, Y. B.; Guo, J. K. *Adv. Funct. Mater.* **2008**, *18*, 2995.

(40) Niu, H. L.; Chen, Q. W.; Ning, M.; Jia, Y. S.; Wang, X. J. *J. Phys. Chem. B* **2004**, *108*, 3998.

(41) Xu, P.; Han, X. J.; Wang, X. H.; Wang, C.; Zhao, H. T.; Zhang, W. J. *Mater. Chem. Phys.* **2008**, *108*, 196.

(42) Nakagawa, N.; Hwang, H. Y.; Muller, D. A. *Nat. Mater.* **2006**, *5*, 204.

(43) Martyna, G. J.; Tuckerman, M. E.; Tobias, D. J.; Klein, M. L. *Mol. Phys.* **1996**, *87*, 1117–1157.

(44) Essmann, U.; Perera, L.; Berkowitz, M. L.; Darden, T.; Lee, H.; Pedersen, L. G. *J. Chem. Phys.* **1995**, *103*, 8577–8593.

JP908839R